THE JOURNAL OF PHYSICAL CHEMISTRY LETTERS
A JOURNAL OF THE AMERICAN CHEMICAL SOCIETY

pubs.acs.org/JPCL Letter

Multiple Magnetic Topological Phases in the van der Waals Crystal $Mn(Bi,Sb)_4Se_7$

Jia-Yi Lin,[‖] Zhong-Jia Chen,[‖] Zhipeng Cao, Jiarui Zeng, Xiao-Bao Yang, Yao Yao, and Yu-Jun Zhao*

Cite This: *J. Phys. Chem. Lett.* 2023, 14, 3913−3919

ABSTRACT: Magnetic topological materials have drawn markedly attention recently due to the strong coupling of their novel topological properties and magnetic configurations. In particular, the $MnBi_2Te_4/(Bi_2Te_3)_n$ family highlights the researches of multiple magnetic topological materials. Via first-principles calculations, we predict that $Mn(Bi, Sb)_4Se_7$, the close relatives of $MnBi_2Te_4/(Bi_2Te_3)_n$ family, are topological nontrivival in both antiferromagnetic and ferromagnetic configurations. In the antiferromagnetic ground state, $Mn(Bi, Sb)_4Se_7$ are simultaneously topological insulators and axion insulators. Massless Dirac surface states emerge on the surfaces parallel to the z axis. In ferromagnetic phases, they are axion insulators. Particularly, when the magnetization direction is along the x axis, they are also topological crystalline insulators. Mirror-symmetry-protected gapless surface states exist on the mirror-invariant surfaces. Hence, the behaviors of surface states are strongly dependent on the magnetization directions and surface orientations. Our work provides more opportunities for the study of magnetic topological physics.

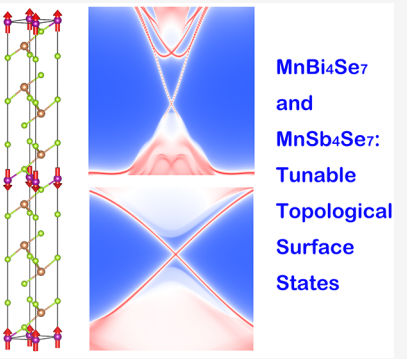

As one of the most fantastic areas of modern condensed matter physics, topological quantum materials have attracted a great deal of interest.[1] Since the early concepts of topological insulators were conceived,[2−4] a series of topological materials of various classes have been proposed theoretically and realized experimentally, such as topological crystalline insulators, Dirac semimetals, Weyl semimetals, and nodal line semimetals.[5−7] The nontrivival band topology guarantees the symmetry-protected surface or hinge states and quasi-particle energy dispersions in these materials. As a result, novel physical properties, such as quantum spin Hall effect, quantum anomalous Hall effect, can be realized on these material platforms.[8,9] Thus, topological states in condensed matter are promising for future dissipationless spintronics devices and quantum computations.[10]

The early discovery of topological materials mostly focuses on the nonmagnetic systems. Typical examples are the Bi_2Se_3 family topological insulators,[11] the SnTe class topological crystalline insulators,[12] the Cd_3As_2 and Na_3Bi Dirac semimetals,[13,14] and the TaAs family Weyl semimetals.[15,16] For the recently developed higher-order band topology, the early condensed mater realization was also in the nonmagnetic platforms.[17,18] This is partially ascribed to the fact that the theoretical calculations for nonmagnetic materials is much more uncomplicated than the magnetic counterparts. Furthermore, the topological quantum chemistry (TQC) and symmetry indicators (SIs) also significantly facilitate the diagnosis of topological materials.[19,20] In the recent days, Vergniory et al.[21] diagnosed all topological bands of all nonmagnetic stoichiometric materials in the Inorganic Crystal Structure Database. It seems that the discovery of topological electronic states in the nonmagnetic materials is tending to be well established.

As for the study of magnetic topological phases, unlike the nonmagnetic counterparts, is still obstructed by lack of sufficient material realizations. The concept model of antiferromagnetic topological insulators was first proposed in 2010.[22] However, the material realization of this topological phase was not achieved until 2019, when $MnBi_2Te_4$ was uncovered.[23] Further study of $MnBi_2Te_4$ confirmed that it is simultaneously an axion insulator in antiferromagnetic state while a Weyl semimetal when tuned to ferromagnetic state.[24] Quantum anomalous Hall effect is also observed in this material.[25] Furthermore, such topological phases, are all strongly coupled to specific magnetic configurations, and thus can be easily tuned and applied to the spintronics devices.[26−28] Such novel performance is impossible to be realized in nonmagnetic materials. Following studies unveil that the $MnBi_2Te_4/(Bi_2Te_3)_n$ (n = 1, 2, 3) are similar tunable magnetic topological materials.[29−35] Topological superconductivity and Majorana edge states were also predicted based on this material family.[36,37]

As a close relative to $MnBi_2Te_4/(Bi_2Te_3)_n$ family, $MnSb_2Te_4/(Sb_2Te_3)_n$ family remains relatively less explored.

Received: January 17, 2023
Accepted: April 14, 2023
Published: April 19, 2023

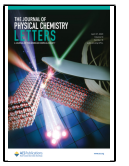

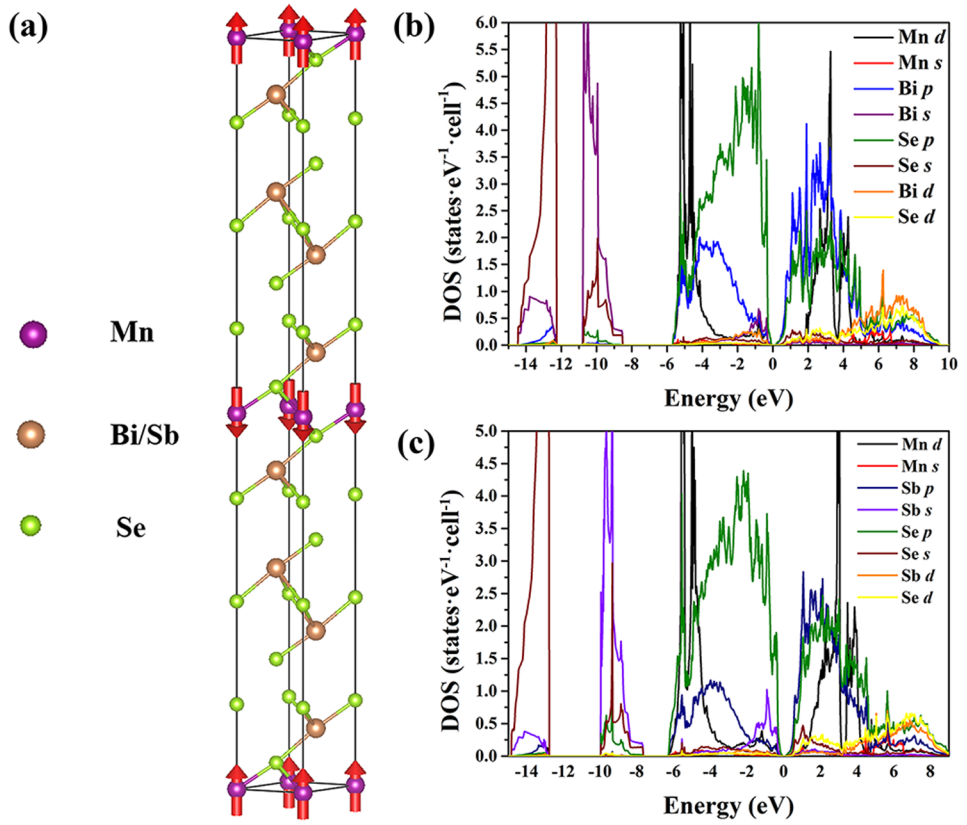

Figure 1. Structures and PDOS of $Mn(Bi, Sb)_4Se_7$. (a) The crystal structure, (b) the PDOS of $MnBi_4Se_7$, and (c) the PDOS of $MnSb_4Se_7$.

The Weyl semimetal state and highly tunable magnetic properties are confirmed in $MnSb_2Te_4$.[38−42] Another highlighted material, $MnSb_4Te_7$, was successfully synthesized by Guo et al.,[43] and a huge anomalous Hall conductivity (AHC) was observed in experiments. It is also expected to be an antiferromagnetic topological insulator and an axion insulator simultaneously in its magnetic ground state. When tuned to the ferromagnetic state with a small external magnetic field, it is an axion insulator regardless of the magnetization direction.[43,44] A ferromagnetic ground state is expected under strain or charge doping.[45] In $Mn_2(Bi, Sb)_2Te_5$ compounds, an antiferromagnetic topological insulator state and a ferromagnetic axion insulator or Weyl semimetal state are predicted.[46−48] The $MnBi_2Se_4$ was discovered to be a high-temperature topological insulator both theoretically and experimentally.[49,50] In view of these emerging exotic phenomenons, it is obvious that more magnetic topological materials with similar structures are desired for the study of topological physics and spintronic applications.

In this work, we predict that $MnBi_4Se_7$ and $MnSb_4Se_7$ are magnetic topological material candidates via first-principles calculations. In their interlayer antiferromagnetic (A-AFM) ground state, they are simultaneously topological insulators and axion insulators with massless Dirac Fermion dispersion emerging on the surfaces parallel to z direction. When turned to ferromagnetic states, they are axion insulators. Furthermore, topological crystalline insulator phases simultaneously emerge when they are magnetized along the x orientation. In this magnetic configuration, mirror-symmetry-protected gapless surface states are expected on their (001) and (010) surfaces. Notably,AHC is expected if these materials are slightly charge doped.

The crystal structure with the calculated magnetic ground state of $Mn(Bi, Sb)_4Se_7$ is shown in Figure 1a. The space group of the primitive cell is $P\bar{3}m1$ (No. 164). It consists of a $Mn(Bi, Sb)_2Se_4$ septuple layer (SL) and a $(Bi, Sb)_2Se_3$ quintuple layer (QL), stacked by van der Waals interaction along z direction. In the paramagnetic state, the magnetic space group is $P\bar{3}m11'$ (No. 164.86) with the group generators as follows:

$$G = \{\hat{E}, \hat{I}, \hat{C}_{3z}, \hat{M}_x\} \otimes \{\hat{E}, \hat{T}\} \quad (1)$$

where $\hat{E}$ stands for the identity operation, $\hat{I}$ for the inversion operation, $\hat{C}_{3z}$ for the 3-fold rotation around z axis, $\hat{M}_x$ for the mirror operation about $x = 0$ plane and $\hat{T}$ for time-reversal operation. In the interlayer antiferromagnetic state (A-AFM), the magnetic space group is $P_c\bar{3}c1$ (No. 165.96) with the generators as follows:

$$G = S \cup \{\hat{T}|\tau_{1/2}\}S \quad (2)$$

where

$$S = \{\hat{E}, \hat{I}, \hat{C}_{3z}, \hat{M}_x\tau_{1/2}\} \quad (3)$$

When magnetized along z direction (FMz), the magnetic space group is $P\bar{3}m'1$ (No. 164.89) with the generators as follows:

$$G = S \cup \{\hat{T}|\hat{M}_x\}S \quad (4)$$

where

$$S = \{\hat{E}, \hat{I}, \hat{C}_{3z}\} \quad (5)$$

When magnetized along x direction (FMx), the magnetic space group is $C2/m$ (No. 12.58) with the generators as follows:

https://doi.org/10.1021/acs.jpclett.3c00162
J. Phys. Chem. Lett. 2023, 14, 3913−3919

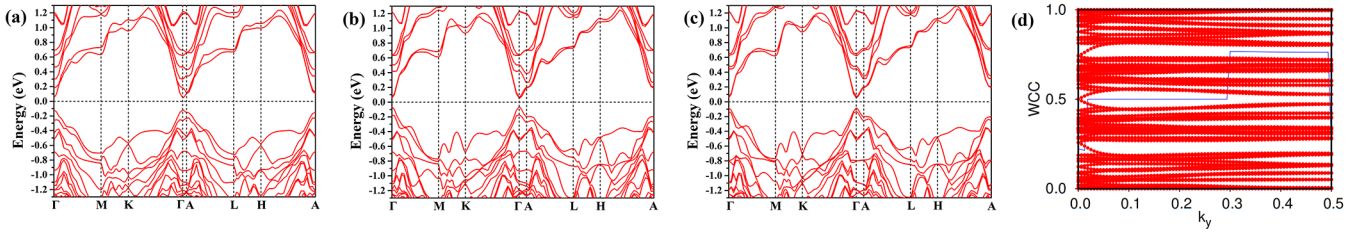

Figure 2. Band structures and Wilson loop of $MnBi_4Se_7$. The band structure of A-AFM magnetic configuration (a), FMz magnetic configuration (b), FMx magnetic configuration (c), and the Wilson loop on the $k_z = 0$ plane of $MnBi_4Se_7$ A-AFM magnetic configuration (d).

$$G = \{\hat{E}, \hat{I}, \hat{M}_x\} \tag{6}$$

When magnetized along y direction (FMy), the magnetic space group is $C2'/m'$ (No. 12.62) with the generators as follows:

$$G = S \cup \{\hat{T}|\hat{M}_x\}S \tag{7}$$

where

$$S = \{\hat{E}, \hat{I}\} \tag{8}$$

The computational details of this work can be found in Section II of Supporting Information. In our calculations, the total energy of FMz is 0.08 meV/Mn lower than the FMx total energy in $MnBi_4Se_7$. In $MnSb_4Se_7$, this value is 0.06 meV/Mn. The total energy of FMy is nearly the same as the FMx total energy in our calculation. The A-AFM total energy is 0.09 meV/Mn lower than the FMz total energy in $MnBi_4Se_7$. In $MnSb_4Se_7$, this value is 0.10 meV/Mn. Based on these values, it seems that 0.032 and 0.035 T external magnetic field are needed to turn A-AFM state to FMz state for $MnBi_4Se_7$ and $MnSb_4Se_7$, respectively. To turn the A-AFM state to the FMx state, 0.061 and 0.057 T external magnetic fields are needed for $MnBi_4Se_7$ and $MnSb_4Se_7$, respectively.

However, it is well-known that the energy scale of the magnetic exchange energy and magnetic anisotropic energy in vdW materials are so small that it reach the accuracy limit of the DFT calculations. Thus, such estimated values may not be consistent with the experimental values. Such problems could be improved by using more accurate but very expensive density functionals, such as hybrid functionals or even GW calculations.

As a comparison, 0.15 T external magnetic field is needed to turn $MnSb_4Te_7$ from A-AFM ground state to FMz state in experiments. We thought the strength of external magnetic field to turn the magnetic states of $MnBi_4Se_7$ and $MnSb_4Se_7$ will not be too large compared to $MnSb_4Te_7$ since the nonmagnetic $(Bi, Sb)_2Se_3$ layers strongly weaken the interlayer magnetic exchange and the Mn 3d bands are slightly far away from the Fermi levels.

As is well-known, the topological properties and the behaviors of surface states are strongly dependent on the symmetries. Thus, there are evident opportunities of tunable magnetic topological properties in $MnBi_4Se_7$ and $MnSb_4Se_7$. Since $MnSb_4Se_7$ has almost the same properties as those of $MnBi_4Se_7$ in our calculations, we choose $MnBi_4Se_7$ as an example for the following discussions.

As shown in Figure 1b,c, the projected density of states (PDOS) of $Mn(Bi, Sb)_4Se_7$ near the valence band maximum (VBM) and conduction band minimum (CBM) are mainly the p orbitals of Bi/Sb and Se, while the Mn 3d orbitals are slightly away from the VBM and CBM. The calculated bulk band structures of $MnBi_4Se_7$ with the A-AFM, FMz, FMx magnetic orders are shown in Figure 2a−c. All the above energy bands open a direct SOC band gap at the Γ point. As for the FMy case, the bulk energy band structure is very similar to the FMx although they have different magnetic space group symmetries.

In $MnBi_4Se_7$, the bulk band gaps for A-AFM, FMz, and FMx are 167.2, 117, and 140.6 meV, respectively. We could understand the origin of the difference of the bulk band gap values in different magnetic configurations as follows. Since these bulk band gaps resulted from the SOC effect, they are quite sensitive to the magnetic configurations with different symmetries. Guaranteed by the $\hat{S} = \hat{T}\tau_{1/2}$ symmetry and inversion symmetry $\hat{I}$, all the bands are double degenerated as Kramer pairs with spin up and spin down states in the A-AFM configuration. When turned to the FM states, such Kramer degeneracy is lifted since the $\hat{S}$ symmetry is broken down. Such band splitting may shift up the VBM and push down the CBM. Then the bulk band gap is reduced in FM states.

The pure spin magnetic moment is 5 μ_B/Mn in $Mn(Bi, Sb)_4Se_7$. However, the orbital magnetic moment can be different when the system is magnetized in different directions. In our calculations, the total magnetic moment is 4.9902 μ_B/Mn for the FMz configuration and 4.9895 μ_B/Mn for the FMx configuration in $MnBi_4Se_7$. In $MnSb_4Se_7$, this value is 4.9975 μ_B/Mn for the FMz configuration and 4.9972 μ_B/Mn for the FMx configuration. This suggests that the orbital magnetic moment in the FMz configuration is smaller than the orbital magnetic moment in the FMx configuration. This plays an important role in the SOC effect and affects the SOC bulk band gap.

In the A-AFM configuration of $MnBi_4Se_7$, since the $\hat{S}$ symmetry and inversion symmetry $\hat{I}$ exist, the band topology of the A-AFM magnetic configuration can be diagnosed by the $\mathbb{Z}_2$ topological invariant:

$$(-1)^{\lambda} = \prod_{k_{inv}, n\in occ/2} \xi_n(k_{inv}) \tag{9}$$

where k_{inv} is the time-reversal invariant k points, n runs over all the occupied Kramers' pairs, and λ is the $\mathbb{Z}_2$ topological invariant. Topological nontrivial $\mathbb{Z}_2 = 1$ is obtained in the $MnBi_4Se_7$ A-AFM configuration, indicating that it is a topological insulator (TI) with quantum spin Hall channels existing on the $\hat{S}$-preserving surfaces. In order to further confirm this feature, we also calculate the Wannier charge center (WCC) on the half of $k_z = 0$ plane of the first Brillouin zone.[51,52] As shown in Figure 2d, the Wilson loop also indicates $\mathbb{Z}_2 = 1$. Since the system has the inversion symmetry, the band topology can also be described by the $\mathbb{Z}_4$ topological symmetry indicator:[53]

https://doi.org/10.1021/acs.jpclett.3c00162
J. Phys. Chem. Lett. 2023, 14, 3913−3919

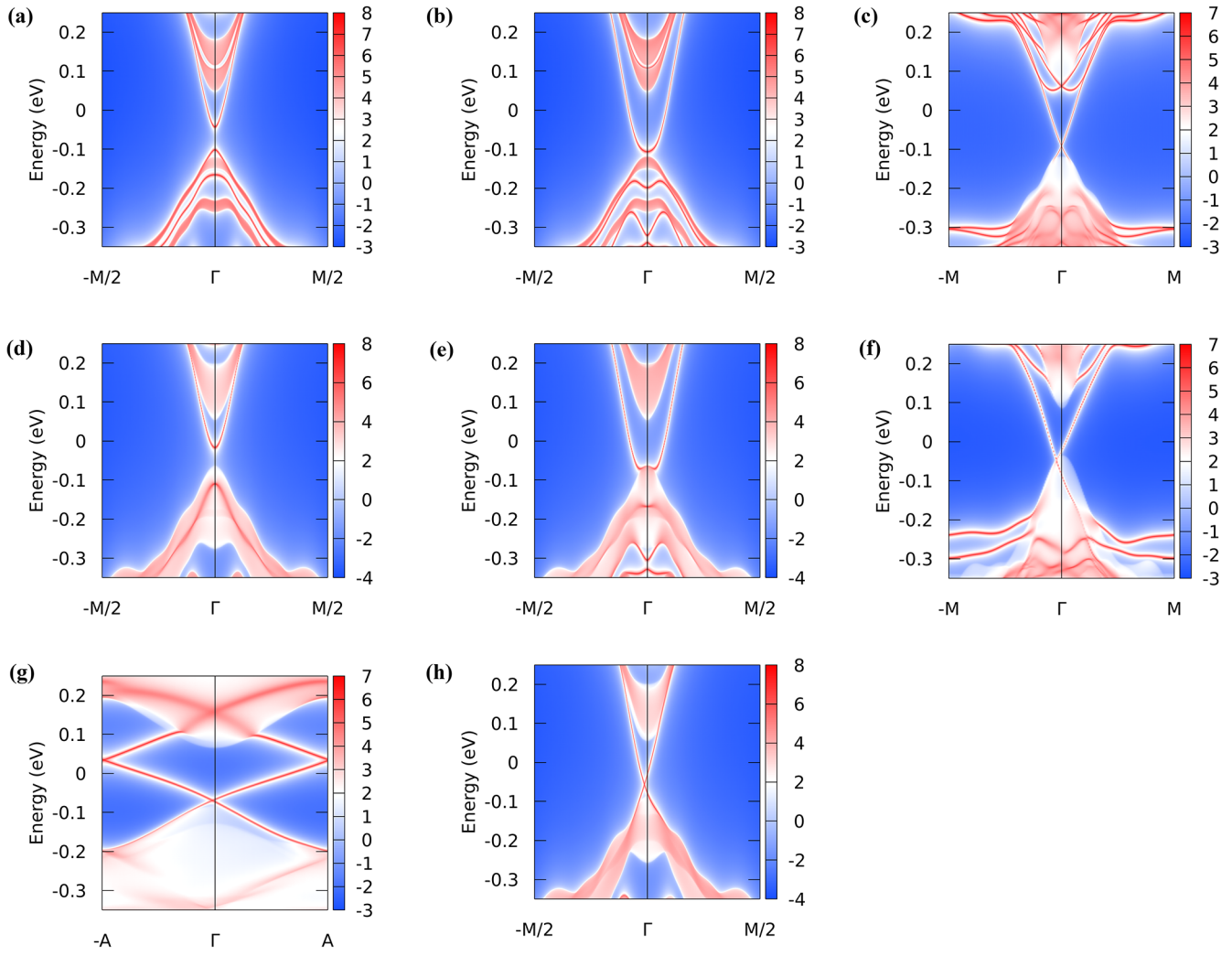

Figure 3. Surface states shown by LDOS confined to the surfaces of $MnBi_4Se_7$. (a) The surface states on (001) surface's QL termination with A-AFM configuration, (b) the SL termination with A-AFM configuration, (c) the massless Dirac Fermion dispersion on the $\hat{S}$-preserving (110) surface with A-AFM configuration, (d) the surface states on (001) surface's QL termination with FM*z* configuration, (e) the SL termination with FM*z* configuration, (f) the surface states on (110) surface with FM*z* configuration, (g) the (010) surface with FM*x* configuration, and (h) the (001) surface's QL termination with FM*x* configuration.

$$\mathbb{Z}_4 = \sum_{\alpha=1}^{8} \sum_{n=1}^{n_{occ}} \frac{1 + \xi_n(\Lambda_\alpha)}{2} \mod 4, \tag{10}$$

where Λ_α is the eight inversion invariant k points in the first Brillouin zone, n runs over all the occupied bands, and $\xi_n(\Lambda_\alpha)$ is the parity eigenvalue of the nth band at Λ_α. It is known that $\mathbb{Z}_4 = 1$ or 3 indicates the topological semimetal phase and $\mathbb{Z}_4 = 2$ indicates the axion insulator (AX) phase. In our calculations, like the $MnSb_4Te_7$ case,[43] $\mathbb{Z}_4 = 2$ is obtained no matter in AFM or FM configurations of $MnBi_4Se_7$. Thus, quantized bulk orbital magnetoelectric coupling is expected in $MnBi_4Se_7$ materials.[54,55]

The bulk-edge correspondence indicates that the nontrivial band topology and inverted band gap give rise to topological surface or hinge states on specific symmetry preserving surfaces or surface boundaries in 3-dimensional topological materials. As for the AFM topological insulators (TI), the gapless topological surface states exist on the $\hat{S}$-symmetry preserving surfaces. In $Mn(Bi, Sb)_4Se_7$ systems, there are two different vdW gap terminations, namely the SL termination and QL termination on the (001) surface. Based on the TB model, we have calculated the local density of states (LDOS) confined to specific surfaces using the iterative Green function method via the WannierTools package to show the surface state spectra.[56] In order to enhance the clarity of projected bulk states, the natural logarithm function is employed for the LDOS and thus negative values are tolerated. As shown in Figure 3a,b, the (001) surface state spectra from the $-M/2$ point (0,−0.25) to the $M/2$ point (0,0.25) in the surface Brillouin zone are all gapped no matter the SL termination or the QL termination in the A-AFM configuration. However, as shown in Figure 3c, the massless Dirac Fermion dispersion is manifested clearly on the $\hat{S}$-preserving (110) surface. Thus, quantum spin Hall chanels are expected theoretically on the $\hat{S}$-preserving surfaces in $MnBi_4Se_7$ of the A-AFM magnetic ground state.

When the system is magnetized to the ferromagnetic configurations, the $\hat{S}$ symmetry is broken down. In the previous discussion, ferromagnetic $MnBi_4Se_7$ is an axion insulator with $\mathbb{Z}_4 = 2$. Generally speaking, the gapped surface state spectrum is more ideal for the experiments to observe the quantized bulk orbital magnetoelectric coupling. In our

https://doi.org/10.1021/acs.jpclett.3c00162
J. Phys. Chem. Lett. 2023, 14, 3913−3919

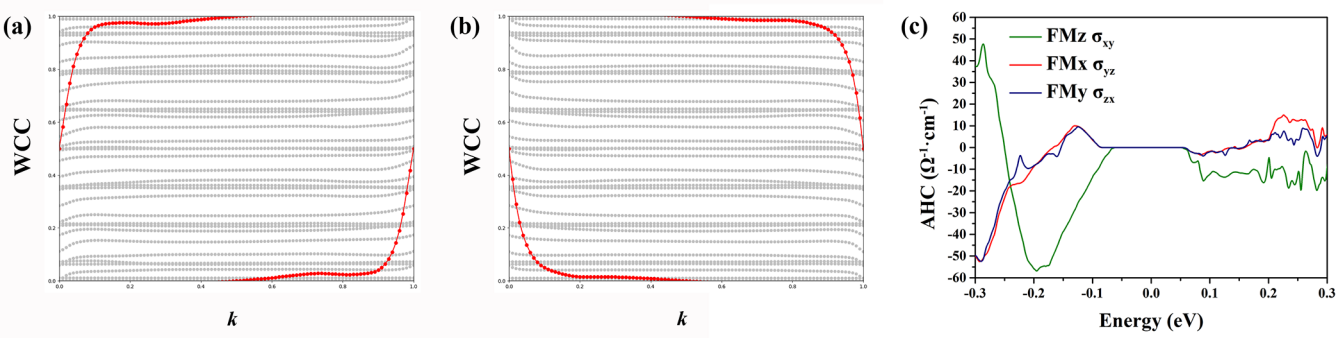

Figure 4. MCNs on the $k_x = 0$ plane with FMx configuration and AHC of $MnBi_4Se_7$. (a) The WCC with mirror eigenvalue $M_x = +i$, (b) the WCC with mirror eigenvalue $M_x = -i$, and (c) the AHC.

calculations, the surface state spectrum of $MnBi_4Se_7$ FM configurations is strongly dependent on the magnetization directions and the surface orientations. In the FMz configuration, as shown in Figure 3d,e, the calculated surface state spectrum is gapped on the QL termination on the (001) surface. However, on the SL termination, the surface state is overlapped with the projected bulk band structure and thus it is gapless. Lacking the $\hat{S}$ symmetry, the surface state spectrum is still degenerated but the degenerate point shifts away from the Γ point on the (110) surface as shown in Figure 3f. It is found that the surface band structures are gapped on other surfaces, such as the (010) surface in the FMz state.

When turned to the in-plane magnetization, things are different. In the FMx configuration, $x = 0$ mirror symmetry exists and plays an important role in the topological property. The calculated SIs indicate that it is a topological crystalline insulator (TCI) with nontrivial mirror Chern numbers (MCNs) $n_{M_x=\pm i} = \pm 1$ defined on the $k_x = 0$ plane in the $+i$ and $-i$ mirror eigenvalue subspaces.[57] As shown in Figure 4(a)(b), the calculated flow of the WCC also confirms $n_{M_x=\pm i} = \pm 1$. Here, the (010) and (001) surfaces are mirror-invariant surfaces. As a consequence of the nontrivival MCNs, gapless surface states are found in their mirror-invariant k-paths on the $k_x = 0$ plane, as shown in Figure 3g,h.

Furthermore, we find that the magnetic topological phases of $MnSb_4Se_7$ are the same as those of $MnBi_4Se_7$ (see Section I of the Supporting Information). Meanwhile, its bulk band structures and surface states are also similar to that of $MnBi_4Se_7$ (see Figure S1 and Figure S2 in the Supporting Information). To better understand the similarities and differences of the $MnBi_4Se_7$, $MnSb_4Se_7$ in this work with the previously reported $MnBi_4Te_7$, $MnSb_4Te_7$, $MnBi_2Se_4$ and $MnSb_2Se_4$, we list their magnetic topological phases in 1 for comparison. Although the TCI phase is not yet reported in $MnBi_4Te_7$ and $MnSb_4Te_7$, we believe this topological phase is possible in these two compounds since they have the same magnetic space group symmetry as the $MnBi_4Se_7$ and $MnSb_4Se_7$ in the FMx configuration.

Table 1. Summary of Topological Phases for $MnBi_4Se_7$, $MnSb_4Se_7$, $MnBi_4Te_7$, $MnSb_4Te_7$, $MnBi_2Se_4$ and $MnSb_2Se_4$[a]

compound	A-AFM	FMz	FMx
$MnBi_4Se_7$	TI and AX	AX	TCI and AX
$MnSb_4Se_7$	TI and AX	AX	TCI and AX
$MnBi_4Te_7$	TI	unreported	unreported
$MnSb_4Te_7$	TI and AX	AX	AX
$MnBi_2Se_4$	TI	Weyl semimetal	Weyl semimetal
$MnSb_2Se_4$	TI	Weyl semimetal	Weyl semimetal

[a]TI, AX, and TCI stand for topological insulator, axion insulator, and topological crystalline insulator, respectively.

Finally, we have calculated the AHC for both $MnBi_4Se_7$ and $MnSb_4Se_7$ in FMz, FMx, and FMy magnetic configurations by the method of Berry curvature:[58]

$$\sigma_{xy} = -\frac{e^2}{\hbar}\int_{BZ}\frac{d^3k}{(2\pi)^3}\Omega^z(\mathbf{k}) \tag{11}$$

where $\Omega^z(\boldsymbol{k})$ is the Berry curvature at $\boldsymbol{k}$ points. The integral runs over all the occupied states in the first Brillouin zone. As shown in Figure 4c and Figure S3c (see Supporting Information), no matter below or above the band gap, notable AHC is expected in these systems when they are magnetized to ferromagnetic states. Such situation is similar to that of the $MnSb_4Te_7$ case. Since the synthesized $MnSb_4Te_7$ sample is slightly hole doped and several Weyl points exist near the Fermi energy, large AHC is measured experimentally by Guo et al. Although no any Weyl node with opposite chirality ±1 is observed between the conduction band and valence band near the Fermi energy in $MnBi_4Se_7$ and $MnSb_4Se_7$, the AHC values are still notable in the charge doped metallic states of these two compounds. Furthermore, since intrinsic defects widely exist in the experimental samples of this material family,[59] such result is also possible in $Mn(Bi,Sb)_4Se_7$ systems. Another way to achieve the charge doping is the gate voltage, which is also a powerful way to drive the magnetic phase transitions experimentally.[60,61]

To draw a conclusion, we have predicted that both $MnBi_4Se_7$ and $MnSb_4Se_7$ are magnetic topological material candidates via first-principles calculations. In the A-AFM magnetic ground state, both are simultaneously antiferromagnetic topological insulators and axion insulators. Massless Dirac Fermion dispersions exist on their $\hat{S}$-symmetry preserving surfaces. When magnetized to ferromagnetic states, they are axion insulators. Furthermore, they are also topological crystalline insulators in the FMx configuration. Mirror-symmetry-protected gapless surface states emerge on their (010) and (001) surfaces. Notable AHC could be expected when these compounds are charge doped. We expect that our work will provide more opportunities for the research of magnetic topological physics.

https://doi.org/10.1021/acs.jpclett.3c00162
J. Phys. Chem. Lett. 2023, 14, 3913−3919

■ ASSOCIATED CONTENT

Data Availability Statement

The data and input files for DFT calculations and source codes for the MCN calculations that support the findings of this study are available upon reasonable request from the authors.

Supporting Information

The Supporting Information is available free of charge at https://pubs.acs.org/doi/10.1021/acs.jpclett.3c00162.

Magnetic topological phases of $MnSb_4Se_7$ and computational details (PDF)

Transparent Peer Review report available (PDF)

■ AUTHOR INFORMATION

Corresponding Author

Yu-Jun Zhao − *Department of Physics, South China University of Technology, Guangzhou 510640, People's Republic of China*; orcid.org/0000-0002-6923-1099; Email: zhaoyj@scut.edu.cn

Authors

Jia-Yi Lin − *Department of Physics, South China University of Technology, Guangzhou 510640, People's Republic of China*

Zhong-Jia Chen − *Songshan Lake Materials Laboratory, Dongguan, Guangdong 523808, China*

Zhipeng Cao − *National Laboratory of Solid State Microstructures and School of Physics, Nanjing University, Nanjing 210093, People's Republic of China; Collaborative Innovation Center of Advanced Microstructures, Nanjing University, Nanjing 210093, People's Republic of China*

Jiarui Zeng − *Department of Physics, South China University of Technology, Guangzhou 510640, People's Republic of China*; orcid.org/0000-0002-5420-3765

Xiao-Bao Yang − *Department of Physics, South China University of Technology, Guangzhou 510640, People's Republic of China*; orcid.org/0000-0001-8851-1988

Yao Yao − *Department of Physics, South China University of Technology, Guangzhou 510640, People's Republic of China*

Complete contact information is available at: https://pubs.acs.org/10.1021/acs.jpclett.3c00162

Author Contributions

‖J.-Y.L. and Z.-J.C. contributed equally to this work

Notes

The authors declare no competing financial interest.

■ ACKNOWLEDGMENTS

This work is financially supported by NSFC (Grant No. 12074126 and No. 12247138), the Foundation for Innovative Research Groups of the National Natural Science Foundation of China (Grant No. 51621001).

■ REFERENCES

(1) Moore, J. E. The Birth of Topological Insulators. *Nature* **2010**, *464*, 194−198.

(2) Haldane, F. D. M. Model for a Quantum Hall Effect without Landau Levels: Condensed-Matter Realization of the "Parity Anomaly. *Phys. Rev. Lett.* **1988**, *61*, 2015−2018.

(3) Kane, C. L.; Mele, E. J. Quantum Spin Hall Effect in Graphene. *Phys. Rev. Lett.* **2005**, *95*, 226801.

(4) Fu, L.; Kane, C. L. Time Reversal Polarization and a Z_2 Adiabatic Spin Pump. *Phys. Rev. B* **2006**, *74*, 195312.

(5) Qi, X.-L.; Zhang, S.-C. Topological Insulators and Superconductors. *Rev. Mod. Phys.* **2011**, *83*, 1057−1110.

(6) Chiu, C.-K.; Teo, J. C. Y.; Schnyder, A. P.; Ryu, S. Classification of Topological Quantum Matter with Symmetries. *Rev. Mod. Phys.* **2016**, *88*, 035005.

(7) Lv, B. Q.; Qian, T.; Ding, H. Experimental Perspective on Three-Dimensional Topological Semimetals. *Rev. Mod. Phys.* **2021**, *93*, 025002.

(8) Bernevig, B. A.; Hughes, T. L.; Zhang, S.-C. Quantum Spin Hall Effect and Topological Phase Transition in HgTe Quantum Wells. *Science* **2006**, *314*, 1757−1761.

(9) Chang, C.-Z.; Zhang, J.; Feng, X.; Shen, J.; Zhang, Z.; Guo, M.; Li, K.; Ou, Y.; Wei, P.; Wang, L.-L.; et al. Experimental Observation of the Quantum Anomalous Hall Effect in a Magnetic Topological Insulator. *Science* **2013**, *340*, 167−170.

(10) Sato, M.; Ando, Y. Topological Superconductors: A Review. *Rep. Prog. Phys.* **2017**, *80*, 076501.

(11) Zhang, H.; Liu, C.-X.; Qi, X.-L.; Dai, X.; Fang, Z.; Zhang, S.-C. Topological Insulators in Bi_2Se_3, Bi_2Te_3 and Sb_2Te_3 with a Single Dirac Cone on the Surface. *Nat. Phys.* **2009**, *5*, 438−442.

(12) Hsieh, T. H.; Lin, H.; Liu, J.; Duan, W.; Bansil, A.; Fu, L. Topological Crystalline Insulators in the SnTe Material Class. *Nat. Commun.* **2012**, *3*, 1−7.

(13) Liu, Z. K.; Jiang, J.; Zhou, B.; Wang, Z. J.; Zhang, Y.; Weng, H. M.; Prabhakaran, D.; Mo, S. K.; Peng, H.; Dudin, P.; et al. A Stable Three-Dimensional Topological Dirac Semimetal Cd_3As_2. *Nat. Mater.* **2014**, *13*, 677−681.

(14) Liu, Z. K.; Zhou, B.; Zhang, Y.; Wang, Z. J.; Weng, H. M.; Prabhakaran, D.; Mo, S.-K.; Shen, Z. X.; Fang, Z.; Dai, X.; et al. Discovery of a Three-Dimensional Topological Dirac Semimetal, Na_3Bi. *Science* **2014**, *343*, 864−867.

(15) Weng, H.; Fang, C.; Fang, Z.; Bernevig, B. A.; Dai, X. Weyl Semimetal Phase in Noncentrosymmetric Transition-Metal Monophosphides. *Phys. Rev. X* **2015**, *5*, 011029.

(16) Lv, B. Q.; Xu, N.; Weng, H. M.; Ma, J. Z.; Richard, P.; Huang, X. C.; Zhao, L. X.; Chen, G. F.; Matt, C. E.; Bisti, F.; et al. Observation of Weyl Nodes in TaAs. *Nat. Phys.* **2015**, *11*, 724−727.

(17) Schindler, F.; Cook, A. M.; Vergniory, M. G.; Wang, Z.; Parkin, S. S. P.; Bernevig, B. A.; Neupert, T. Higher-Order Topological Insulators. *Sci. Adv.* **2018**, *4*, No. eaat0346.

(18) Schindler, F.; Wang, Z.; Vergniory, M. G.; Cook, A. M.; Murani, A.; Sengupta, S.; Kasumov, A. Y.; Deblock, R.; Jeon, S.; Drozdov, I.; et al. Higher-Order Topology in Bismuth. *Nat. Phys.* **2018**, *14*, 918−924.

(19) Bradlyn, B.; Elcoro, L.; Cano, J.; Vergniory, M. G.; Wang, Z.; Felser, C.; Aroyo, M. I.; Bernevig, B. A. Topological Quantum Chemistry. *Nature* **2017**, *547*, 298−305.

(20) Tang, F.; Po, H. C.; Vishwanath, A.; Wan, X. Comprehensive Search for Topological Materials Using Symmetry Indicators. *Nature* **2019**, *566*, 486−489.

(21) Vergniory, M. G.; Wieder, B. J.; Elcoro, L.; Parkin, S. S. P.; Felser, C.; Bernevig, B. A.; Regnault, N. All Topological Bands of All Nonmagnetic Stoichiometric Materials. *Science* **2022**, *376*, No. eabg9094.

(22) Mong, R. S. K.; Essin, A. M.; Moore, J. E. Antiferromagnetic Topological Insulators. *Phys. Rev. B* **2010**, *81*, 245209.

(23) Otrokov, M. M.; Klimovskikh, I. I.; Bentmann, H.; Estyunin, D.; Zeugner, A.; Aliev, Z. S.; Gaß, S.; Wolter, A. U. B.; Koroleva, A. V.; Shikin, A. M.; et al. Prediction and Observation of an Antiferromagnetic Topological Insulator. *Nature* **2019**, *576*, 416−422.

(24) Zhang, D.; Shi, M.; Zhu, T.; Xing, D.; Zhang, H.; Wang, J. Topological Axion States in the Magnetic Insulator $MnBi_2Te_4$ with the Quantized Magnetoelectric Effect. *Phys. Rev. Lett.* **2019**, *122*, 206401.

(25) Deng, Y.; Yu, Y.; Shi, M. Z.; Guo, Z.; Xu, Z.; Wang, J.; Chen, X. H.; Zhang, Y. Quantum Anomalous Hall Effect in Intrinsic Magnetic Topological Insulator $MnBi_2Te_4$. *Science* **2020**, *367*, 895−900.

(26) Yang, Z.; Zhang, H. Evolution of Surface States of Antiferromagnetic Topological Insulator $MnBi_2Te_4$ with Tuning the Surface Magnetization. *New J. Phys.* **2022**, *24*, 073034.
(27) Lei, C.; MacDonald, A. H. Gate-Tunable Quantum Anomalous Hall Effects in $MnBi_2Te_4$ Thin Films. *Phys. Rev. Materials* **2021**, *5*, L051201.
(28) Padmanabhan, H.; Stoica, V. A.; Kim, P. K.; Poore, M.; Yang, T.; Shen, X.; Reid, A. H.; Lin, M.-F.; Park, S.; Yang, J.; et al. Large Exchange Coupling Between Localized Spins and Topological Bands in Magnetic Topological Insulator $MnBi_2Te_4$. *Adv. Mater.* **2022**, *34*, 2202841.
(29) Hu, C.; Gordon, K. N.; Liu, P.; Liu, J.; Zhou, X.; Hao, P.; Narayan, D.; Emmanouilidou, E.; Sun, H.; Liu, Y.; et al. A van der Waals Antiferromagnetic Topological Insulator with Weak Interlayer Magnetic Coupling. *Nat. Commun.* **2020**, *11*, 1−8.
(30) Guan, Y. D.; Yan, C. H.; Lee, S. H.; Gui, X.; Ning, W.; Ning, J. L.; Zhu, Y. L.; Kothakonda, M.; Xu, C. Q.; Ke, X. L.; et al. Ferromagnetic $MnBi_4Te_7$ Obtained with Low-Concentration Sb Doping: A Promising Platform for Exploring Topological Quantum States. *Phys. Rev. Materials* **2022**, *6*, 054203.
(31) Vidal, R. C.; et al. Orbital Complexity in Intrinsic Magnetic Topological Insulators $MnBi_4Te_7$ and $MnBi_6Te_{10}$. *Phys. Rev. Lett.* **2021**, *126*, 176403.
(32) Tian, S.; et al. Magnetic Topological Insulator $MnBi_6Te_{10}$ with a Zero-Field Ferromagnetic State and Gapped Dirac Surface States. *Phys. Rev. B* **2020**, *102*, 035144.
(33) Lu, R.; et al. Half-Magnetic Topological Insulator with Magnetization-Induced Dirac Gap at a Selected Surface. *Phys. Rev. X* **2021**, *11*, 011039.
(34) Hu, C.; Ding, L.; Gordon, K. N.; Ghosh, B.; Tien, H.-J.; Li, H.; Linn, A. G.; Lien, S.-W.; Huang, C.-Y.; Mackey, S.; et al. Realization of an Intrinsic Ferromagnetic Topological State in $MnBi_8Te_{13}$. *Sci. Adv.* **2020**, *6*, No. eaba4275.
(35) Deng, H.; Chen, Z.; Wołoś, A.; Konczykowski, M.; Sobczak, K.; Sitnicka, J.; Fedorchenko, I. V.; Borysiuk, J.; Heider, T.; Pluciński, Ł.; et al. High-Temperature Quantum Anomalous Hall Regime in a $MnBi_2Te_4/Bi_2Te_3$ Superlattice. *Nat. Phys.* **2021**, *17*, 36−42.
(36) Wang, L.; Shi, Y.; Liu, M.; Zhang, A.; Hong, Y.-L.; Li, R.; Gao, Q.; Chen, M.; Ren, W.; Cheng, H.-M.; et al. Intercalated Architecture of MA_2Z_4 Family Layered van der Waals Materials with Emerging Topological, Magnetic and Superconducting Properties. *Nat. Commun.* **2021**, *12*, 1−10.
(37) Zhang, X.; Liu, F. Prediction of Majorana Edge States from Magnetized Topological Surface States. *Phys. Rev. B* **2021**, *103*, 024405.
(38) Yin, Y.; Ma, X.; Yan, D.; Yi, C.; Yue, B.; Dai, J.; Zhao, L.; Yu, X.; Shi, Y.; Wang, J.-T.; Hong, F. Pressure-Driven Electronic and Structural Phase Transition in Intrinsic Magnetic Topological Insulator $MnSb_2Te_4$. *Phys. Rev. B* **2021**, *104*, 174114.
(39) Zhou, L.; Tan, Z.; Yan, D.; Fang, Z.; Shi, Y.; Weng, H. Topological Phase Transition in the Layered Magnetic Compound $MnSb_2Te_4$: Spin-Orbit Coupling and Interlayer Coupling Dependence. *Phys. Rev. B* **2020**, *102*, 085114.
(40) Zang, Z.; et al. Layer-Number-Dependent Antiferromagnetic and Ferromagnetic Behavior in $MnSb_2Te_4$. *Phys. Rev. Lett.* **2022**, *128*, 017201.
(41) Liu, Y.; Wang, L.-L.; Zheng, Q.; Huang, Z.; Wang, X.; Chi, M.; Wu, Y.; Chakoumakos, B. C.; McGuire, M. A.; Sales, B. C.; et al. Site Mixing for Engineering Magnetic Topological Insulators. *Phys. Rev. X* **2021**, *11*, 021033.
(42) Rodriguez-Vega, M.; Lin, Z.-X.; Leonardo, A.; Ernst, A.; Vergniory, M. G.; Fiete, G. A. Light-Driven Topological and Magnetic Phase Transitions in Thin Layer Antiferromagnets. *J. Phys. Chem. Lett.* **2022**, *13*, 4152−4158.
(43) Huan, S.; Zhang, S.; Jiang, Z.; Su, H.; Wang, H.; Zhang, X.; Yang, Y.; Liu, Z.; Wang, X.; Yu, N.; et al. Multiple Magnetic Topological Phases in Bulk van der Waals Crystal $MnSb_4Te_7$. *Phys. Rev. Lett.* **2021**, *126*, 246601.
(44) Eremeev, S. V.; Rusinov, I. P.; Koroteev, Y. M.; Vyazovskaya, A. Y.; Hoffmann, M.; Echenique, P. M.; Ernst, A.; Otrokov, M. M.; Chulkov, E. V. Topological Magnetic Materials of the $(MnSb_2Te_4)\cdot(Sb_2Te_3)_n$ van der Waals Compounds Family. *J. Phys. Chem. Lett.* **2021**, *12*, 4268−4277.
(45) Lin, J.-Y.; Chen, Z.-J.; Xie, W.-Q.; Yang, X.-B.; Zhao, Y.-J. Toward Ferromagnetic Semimetal Ground State with Multiple Weyl Nodes in van der Waals Crystal $MnSb_4Te_7$. *New J. Phys.* **2022**, *24*, 043033.
(46) Li, Y.; Jiang, Y.; Zhang, J.; Liu, Z.; Yang, Z.; Wang, J. Intrinsic Topological Phases in $Mn_2Bi_2Te_5$ Tuned by the Layer Magnetization. *Phys. Rev. B* **2020**, *102*, No. 121107.
(47) Cao, L.; Han, S.; Lv, Y.-Y.; Wang, D.; Luo, Y.-C.; Zhang, Y.-Y.; Yao, S.-H.; Zhou, J.; Chen, Y. B.; Zhang, H.; Chen, Y.-F. Growth and Characterization of the Dynamical Axion Insulator Candidate $Mn_2Bi_2Te_5$ with Intrinsic Antiferromagnetism. *Phys. Rev. B* **2021**, *104*, 054421.
(48) Eremeev, S. V.; Otrokov, M. M.; Ernst, A.; Chulkov, E. V. Magnetic Ordering and Topology in $Mn_2Bi_2Te_5$ and $Mn_2Sb_2Te_5$ van der Waals Materials. *Phys. Rev. B* **2022**, *105*, 195105.
(49) Zhu, T.; Bishop, A. J.; Zhou, T.; Zhu, M.; O'Hara, D. J.; Baker, A. A.; Cheng, S.; Walko, R. C.; Repicky, J. J.; Liu, T.; et al. Synthesis, Magnetic Properties, and Electronic Structure of Magnetic Topological Insulator $MnBi_2Se_4$. *Nano Lett.* **2021**, *21*, 5083−5090.
(50) Zhang, H.; Yang, W.; Wang, Y.; Xu, X. Tunable Topological States in Layered Magnetic Materials of $MnSb_2Te_4$, $MnBi_2Se_4$, and $MnSb_2Se_4$. *Phys. Rev. B* **2021**, *103*, 094433.
(51) Yu, R.; Qi, X. L.; Bernevig, A.; Fang, Z.; Dai, X. Equivalent Expression of Z_2 Topological Invariant for Band Insulators Using the Non-Abelian Berry Connection. *Phys. Rev. B* **2011**, *84*, 075119.
(52) Soluyanov, A. A.; Vanderbilt, D. Wannier Representation of Z_2 Topological Insulators. *Phys. Rev. B* **2011**, *83*, 035108.
(53) Xu, Y.; Song, Z.; Wang, Z.; Weng, H.; Dai, X. Higher-Order Topology of the Axion Insulator $EuIn_2As_2$. *Phys. Rev. Lett.* **2019**, *122*, 256402.
(54) Essin, A. M.; Moore, J. E.; Vanderbilt, D. Magnetoelectric Polarizability and Axion Electrodynamics in Crystalline Insulators. *Phys. Rev. Lett.* **2009**, *102*, 146805.
(55) Malashevich, A.; Souza, I.; Coh, S.; Vanderbilt, D. Theory of Orbital Magnetoelectric Response. *New J. Phys.* **2010**, *12*, 053032.
(56) Sancho, M. P. L.; Sancho, J. M. L.; Sancho, J. M. L.; Rubio, J. Highly Convergent Schemes for the Calculation of Bulk and Surface Green Functions. *Journal of Physics F: Metal Physics* **1985**, *15*, 851.
(57) Peng, B.; Jiang, Y.; Fang, Z.; Weng, H.; Fang, C. Topological Classification and Diagnosis in Magnetically Ordered Electronic Materials. *Phys. Rev. B* **2022**, *105*, 235138.
(58) Yao, Y.; Kleinman, L.; MacDonald, A. H.; Sinova, J.; Jungwirth, T.; Wang, D.-s.; Wang, E.; Niu, Q. First Principles Calculation of Anomalous Hall Conductivity in Ferromagnetic bcc Fe. *Phys. Rev. Lett.* **2004**, *92*, 037204.
(59) Du, M.-H.; Yan, J.; Cooper, V. R.; Eisenbach, M. Tuning Fermi Levels in Intrinsic Antiferromagnetic Topological Insulators $MnBi_2Te_4$ and $MnBi_4Te_7$ by Defect Engineering and Chemical Doping. *Adv. Funct. Mater.* **2021**, *31*, 2006516.
(60) Zheng, G.; Xie, W.-Q.; Albarakati, S.; Algarni, M.; Tan, C.; Wang, Y.; Peng, J.; Partridge, J.; Farrar, L.; Yi, J.; et al. Gate-Tuned Interlayer Coupling in van der Waals Ferromagnet Fe_3GeTe_2 Nanoflakes. *Phys. Rev. Lett.* **2020**, *125*, 047202.
(61) Tan, C.; Xie, W.-Q.; Zheng, G.; Aloufi, N.; Albarakati, S.; Algarni, M.; Li, J.; Partridge, J.; Culcer, D.; Wang, X.; et al. Gate-Controlled Magnetic Phase Transition in a van der Waals Magnet Fe_5GeTe_2. *Nano Lett.* **2021**, *21*, 5599−5605.

https://doi.org/10.1021/acs.jpclett.3c00162
J. Phys. Chem. Lett. 2023, 14, 3913−3919